Supporting Information

Argyrodite Solid Electrolyte with Stable Interface and Superior Dendrite Suppression Capability Realized by ZnO Co-doping

Ting Chen,[1] Long Zhang,[1,*] Zhaoxing Zhang,[1] Peng Li,[1] Hongqiang Wang,[2] Chuang Yu,[3] Xinlin Yan,[4] Limin Wang,[1] Bo Xu[1]

[1]Clean Nano Energy Center, State Key Laboratory of Metastable Materials Science and Technology, Yanshan University, Qinhuangdao, Hebei 066004, China

[2]College of Chemistry & Environmental Science, Hebei University, Baoding, Hebei 071000, China

[3]Department of Mechanical and Materials Engineering, University of Western Ontario, 1151 Richmond St, London, Ontario, N6A 3K7, Canada

[4]Institute of Solid State Physics, Vienna University of Technology, Wiedner Hauptstr. 8-10, 1040 Vienna, Austria

*E-mail: lzhang@ysu.edu.cn

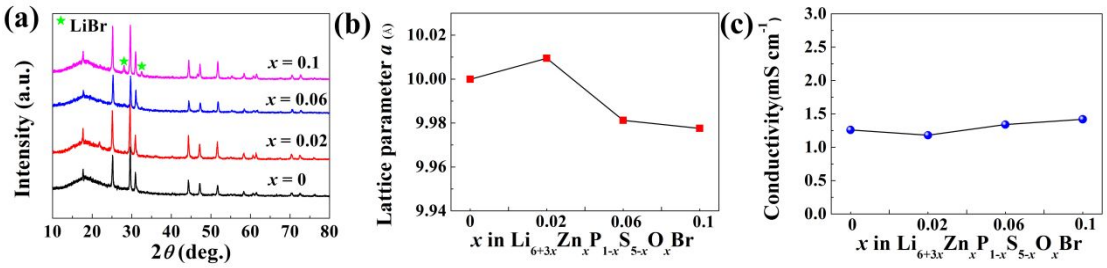

Figure S1. Zn dopes on the P sites instead of the Li sites. (a) XRD patterns of $Li_{6+3x}Zn_xP_{1-x}S_{5-x}O_xBr$ ($0 \leq x \leq 0.1$). (b) Compositional dependence of the lattice parameter for $Li_{6+3x}Zn_xP_{1-x}S_{5-x}O_xBr$ (x = 0, 0.02, 0.06, 0.1). (c) Composition dependent room temperature ionic conductivity for $Li_{6+3x}Zn_xP_{1-x}S_{5-x}O_xBr$ ($0 \leq x \leq 0.1$).

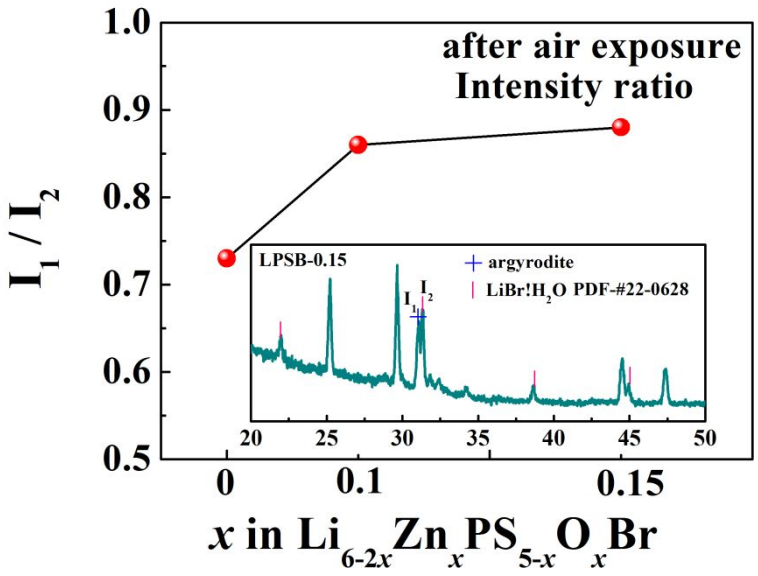

Figure S2. Intensity ratio of the argyrodite phase to the impurity LiBr!H_2O (I_1/I_2) for $Li_{6-2x}Zn_xPS_{5-x}O_xBr$ (x = 0, 0.1, 0.15) exposed in air with ~70% humidity for 10 min. The inset show the representative XRD profile of LPSB-0.15.

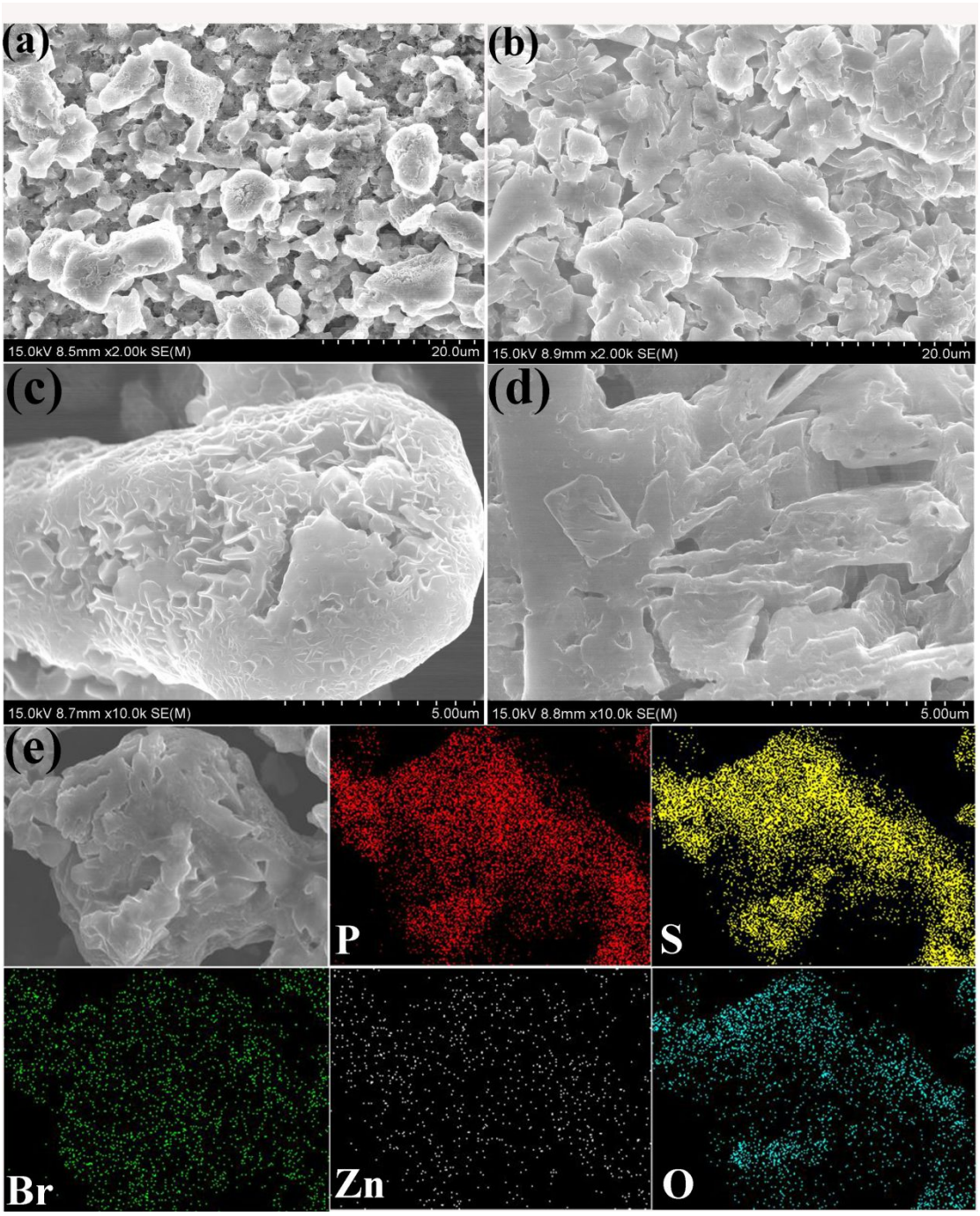

Figure S3. SEM images of the LPSB powders (a, c) and the LPSB-0.15 powders (b, d). (e) EDX mapping of P, S, Br, Zn, and O elements for LPSB-0.15.

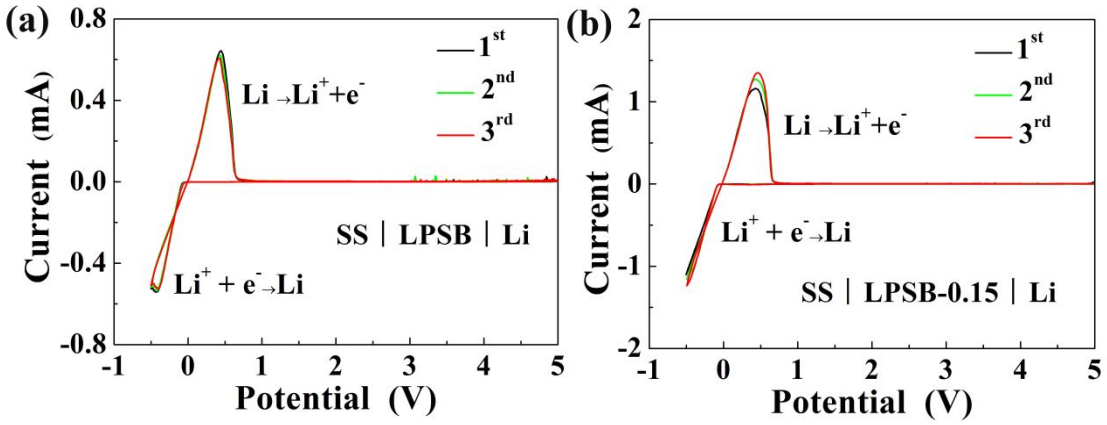

Figure S4. Cyclic voltammograms of LPSB and LPSB-0.15 electrolytes.

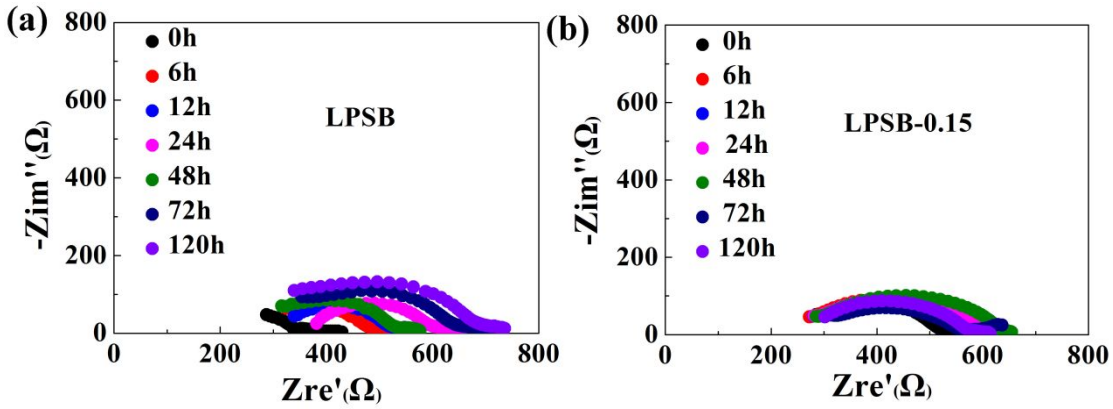

Figure S5. Nyquist plots of the Li/electrolyte/Li symmetric cells with LPSB (a) and LPSB-0.15 (b) electrolytes as a function of storage time at room temperature.

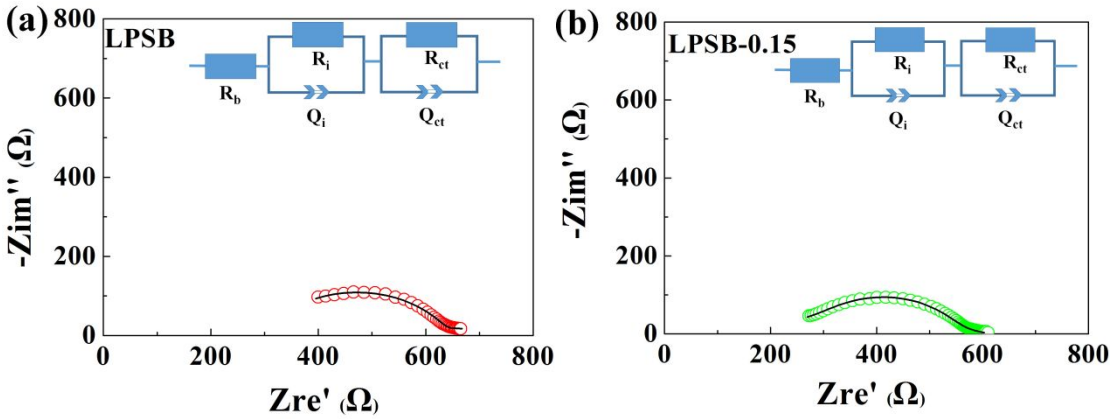

Figure S6. Selected Nyquist plots of the Li/electrolyte/Li symmetric cells with LPSB (a) and LPSB-0.15 (b) electrolytes after contacting with Li for 72 h. The solid line represents the fitting curve with the equivalent circuit shown in the inset.

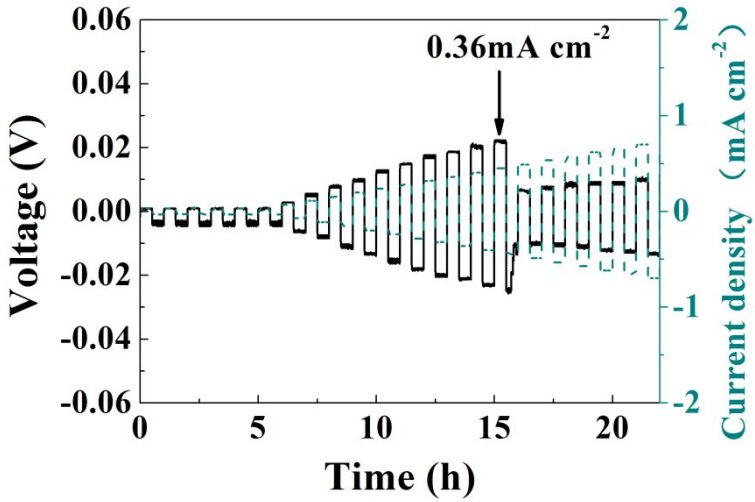

Figure S7. Galvanostatic intermittent cycling of Li/LPSB/Li symmetric cells at step-increased current densities at room temperature.

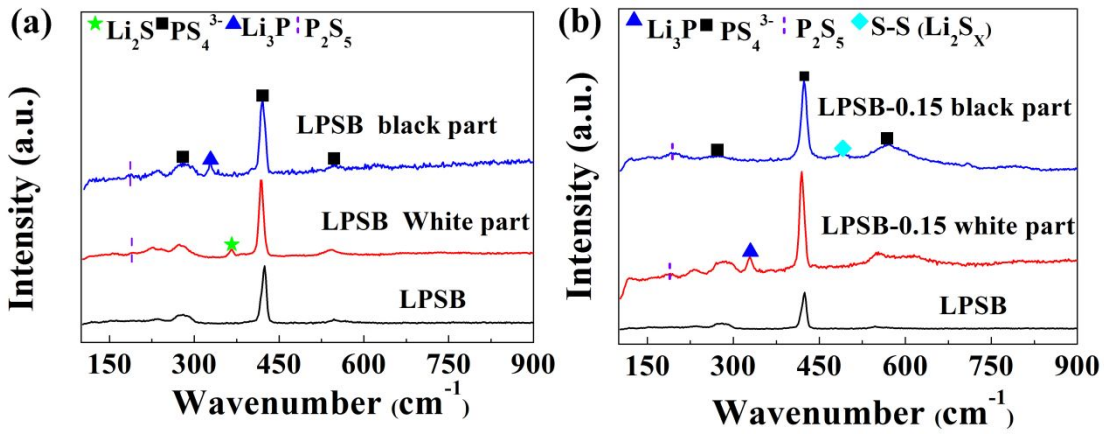

Figure S8. Raman spectra of the SE/Li interface on the Li/Li symmetric cells with LPSB (a) and LPSB-0.15 (b) electrolytes after polarization tests.

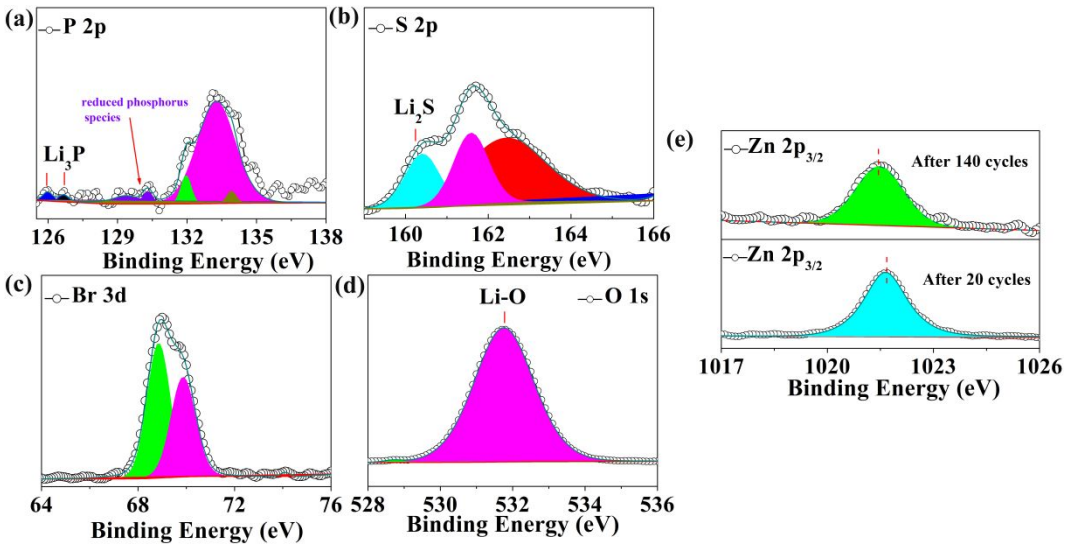

Figure S9. XPS spectra of P 2p (a), S 2p (b), Br 3d (c), and O 1s (d) for LPSB-0.15 electrolyte after polarization cycling on a Li/LPSB-0.15/Li symmetric cell for 140 cycles. (e) XPS spectrum of Zn $2p_{3/2}$ for LPSB-0.15 electrolyte after polarization cycling for 140 cycles (upper panel) and 20 cycles (lower panel), respectively.

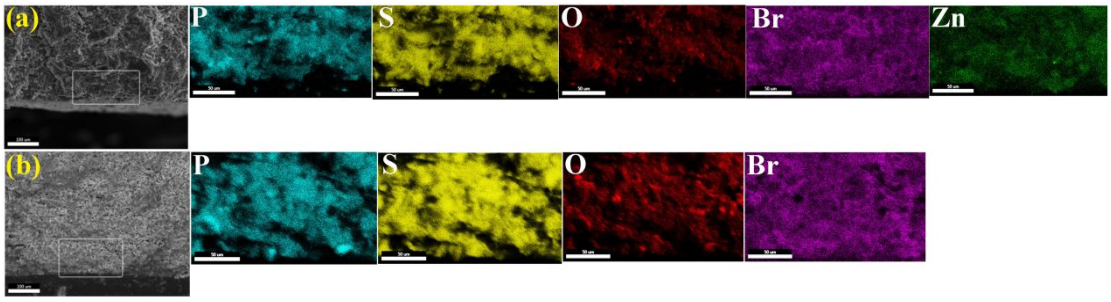

Figure S10. The cross-sectional SEM images and the corresponding elemental mapping of the cold-pressed LPSB (a) and LPSB-0.15 (b) electrolytes.

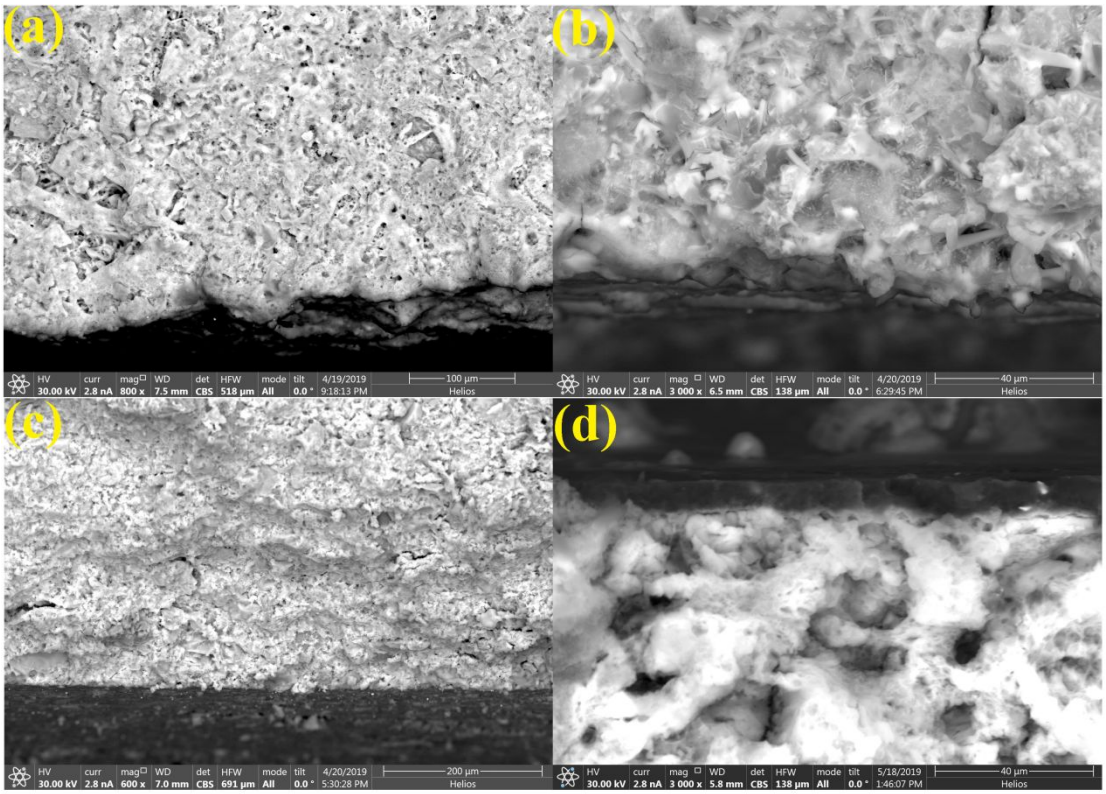

Figure S11. CBS images of LPSB (a, b) and LPSB-0.15 (c, d) electrolytes after galvanostatic polarization cycling.

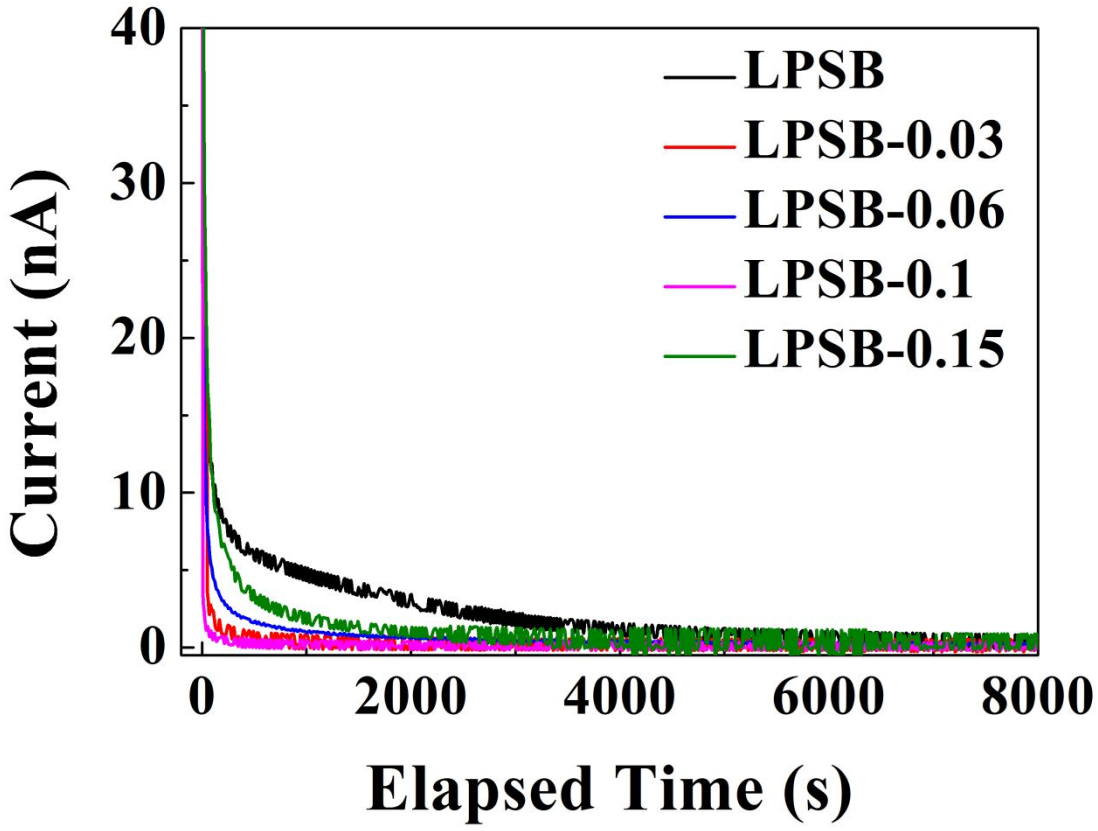

Figure S12. DC polarization current as a function of time with a constant voltage of 1 V tested on the SS/$Li_{6-2x}Zn_xPS_{5-x}O_xBr$ (x = 0, 0.03, 0.06, 0.1, 0.15)/SS cells.

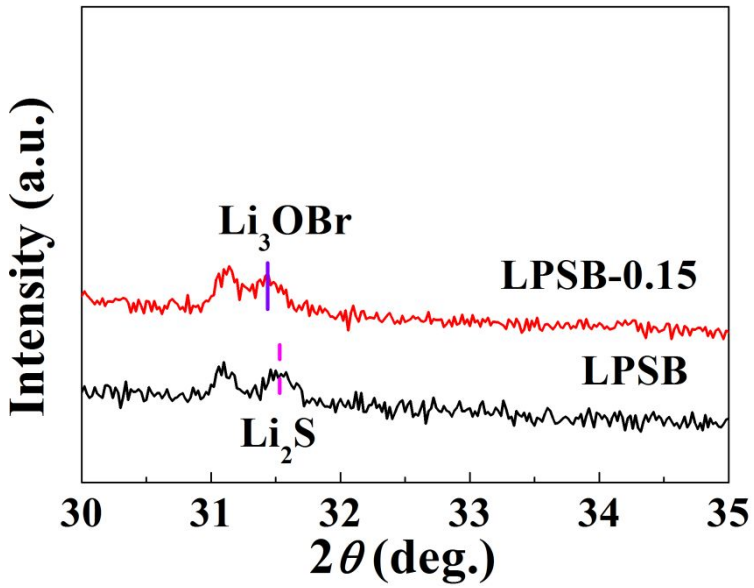

Figure S13. Magnification of the XRD patterns shown in Figure 4b, c to illustrate the different decomposition products (Li_3OBr and Li_2S).

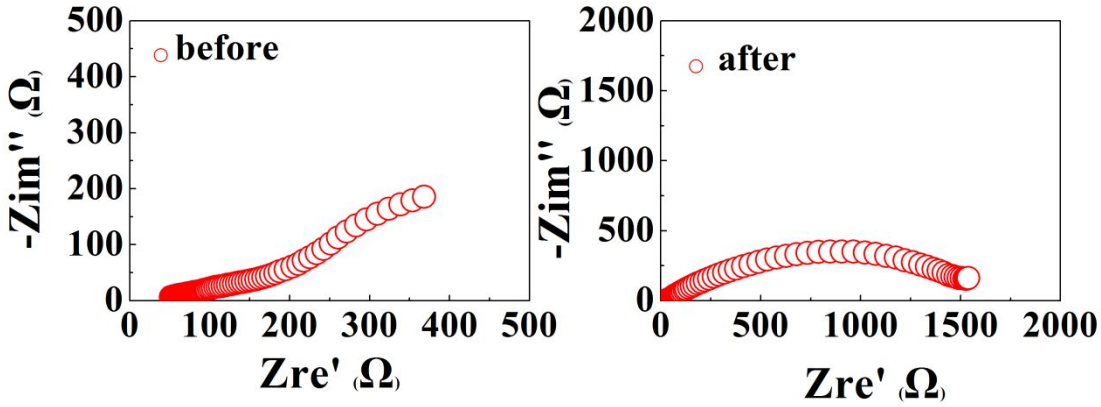

Figure S14. Impedance spectra of NCM-811/LPSB/Li-In cell before and after cycling.

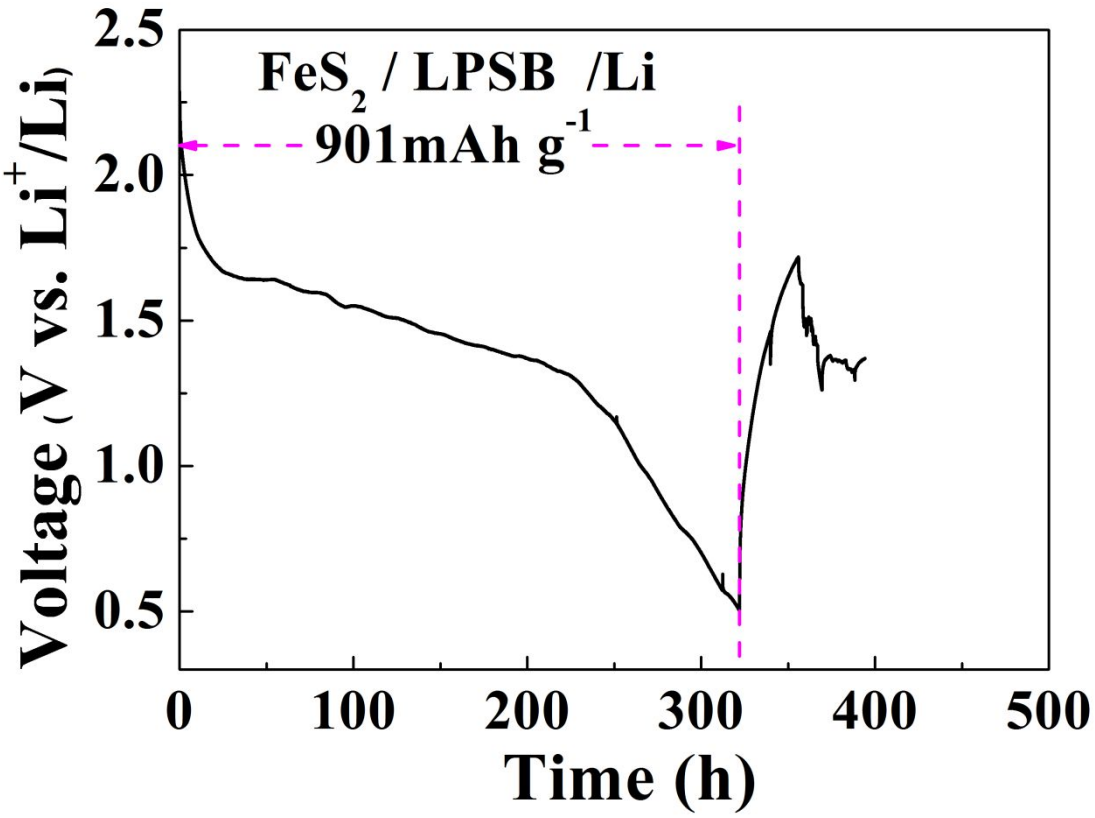

Figure S15. Voltage profiles of the FeS_2/LPSB/Li cell. This cell with ZnO-free LPSB electrolyte cannot run even for one cycle.

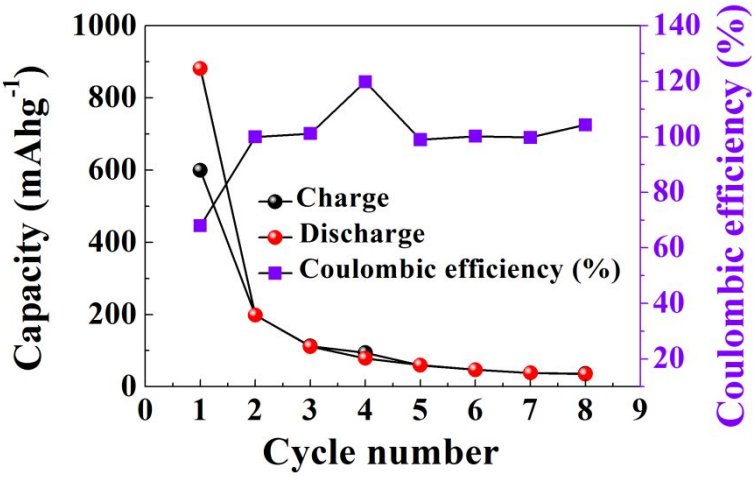

Figure S16. Cycling performance of the FeS_2/LPSB-0.15/Li cell.